Conference Paper, Published Version

Jones, Sterling J.

Indirect Methods of Measuring Shear Stress in the Bottom of a Scour Hole

Indirect Methods of Measuring Shear Stress in the Bottom of a Scour Hole

By
J. Sterling Jones

INTRODUCTION

Most rational methods for estimating scour in cohesive or consolidated bed materials are time dependent and are in terms of excess shear stress or excess stream power. To apply the logic of these methodologies to the bridge pier scour problem one would need to somehow determine the shear stress or stream power in the scour hole as a function of the depth of the scour hole. The challenge, for scour evaluations to link with the technology that has evolved from erosion research, is to find a way to track the maximum shear stress in the scour hole.
The magnitude of the approach flow shear stress is amplified several fold at the beginning of scour but it decays as the scour hole gets deeper. Shear stress is a very logical concept, but it is very difficult to measure even in a laboratory. Engineers typically compute shear stresses based on fully developed normal flow or on an assumed ideal velocity distribution. The highly complex flow patterns around a bridge pier are anything but either of these conditions as illustrated by the flow visualization photo in figure 1. Direct measuring devices such as dynamometers designed to measure a drag force on a small element of the channel bed and shear stress pads which measure the velocity gradient near the bed probably do not capture the effects of the diving currents and vortices that are primarily responsible for dislodging the particles that are scoured out of the scour hole. Even sophisticated 3-D models, which can generate a shear stress for any element in the flow field, probably do not reflect the erodibility effects of the diving currents and vortices that dominate of the scour process unless they have been calibrated for those kind of secondary currents.

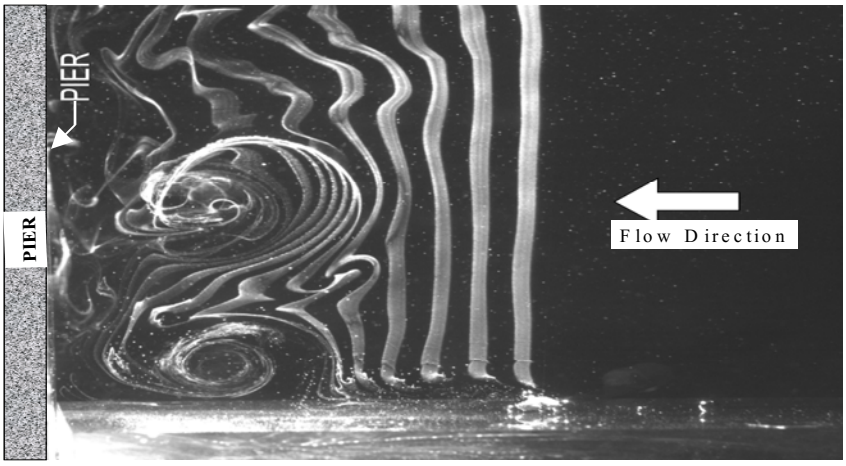

Figure 1. Photo of Visualized Flow in Front of a Bridge Pier

When researchers at the FHWA TFHRC Hydraulics laboratory were confronted with the problem of finding a practical way of determining shear stresses around bridge piers, a

number of alternatives were considered. One was a calibrated shear stress hemisphere which was an assortment of small hemispheres that could be placed anywhere along the bed. The idea was to keep exchanging hemispheres to find the one that just barely moved and that one would be an indirect measure of the shear stress at that point. Dr. Peggy Johnson, who was working at the lab at that time, reasoned that we could accomplish almost the same thing by using different size sand particles by running experiments long enough to reach the point that the sand particles were barely moving. Based on that logic, researchers at the lab embarked on an experimental program of long duration scour tests to indirectly measure effective shear stresses and stream power in scour holes at different. depths. The key word in that endeavor was ”effective” because we were really trying to characterize all the forces that act on a particle to dislodge it as a single parameter that could be related to the shear stress in the approach flow where the typical assumptions for computing shear stress are valid.

We published a technical paper based on this study in the proceedings of the ASCE Water Resources Conference’98 held in Memphis TN.(1) That paper documented the technique used to extrapolate shorter duration runs to predict equilibrium scour for a much longer duration run, but it did not document the process used to develop shear stress ratios that are the key to coupling erosion concepts with scour computations.

Previous Studies

Johnson conducted a study using marbles to indirectly measure shear stress at the base of piers at various preformed scour depths.(2) Marbles make a convenient particle for sediment studies because they have approximately the same specific gravity as granite sand and they are very uniform in size. The problem with marbles is they roll by themselves unless they are packed against one another. Johnson concluded that the effective shear stress at the base of a pier varied from 2.8 to 1.4 times the shear stress in the approach flow depending on the depth of scour.

Parola conducted a study of riprap sizes necessary to protect bridge piers against scour. (3) He used gravel particles to indirectly determine the effective velocity at the base of a pier. He compared the approach velocity required to move a particle at the base of a pier to the velocity that would be required to move the same size particle in unobstructed flow and concluded that the effective velocity at the base of a pier must be approximately 1.5 to 1.7 times the approach velocity. Since shear stress is related to velocity squared, it follows that Parola’s effective shear stress was 2.2 to 2.9 times the shear stress in the approach.

Pagan conducted a similar study of riprap protection for bridge abutments and found that the effective velocity at the base of abutments must be approximately two times the average contracted velocity through the bridge opening; hence his maximum effective shear stresses at the base of abutments represented an amplification of approximately four times the average shear stress in the contracted section.(4)

Both Parola and Pagan were looking at the amplification factor for zero scour depth, but Johnson did attempt to determine the decay rate as the scour hole got deeper.

to reach an equilibrium depth for clear water experiments, the *effective* shear stress in the bottom of the scour hole must have reached critical for that sediment size.

The experiments were designed to determine how much the approach flow shear stress is effectively amplified at the base of a pier as a function of the local scour depth. Each experiment provided one point on a shear stress amplification curve where the approach flow shear stress (always equal or less than critical for the sediment size) could be computed from the velocity and flow depth, the shear stress at the base of the pier could be computed as the critical shear stress for the sediment size, from Shields or other similar criteria, and the equilibrium scour depth was a measured quantity. The sediment particles themselves were indirectly measuring all the forces acting to cause motion in the complicated flow field around the pier. The combined effects of these forces could be represented as an effective shear stress that is comparable to the shear stress that is associated with one-dimensional flow such as the flow past a sediment sample in the Texas A&M erosion function apparatus (EFA).
The primary procedural issue in running these experiments was how long to run each test so that the equilibrium scour depth could be estimated with reasonable confidence. Theoretically clear water scour never reaches equilibrium but is asymptotic with time, but most of the scour occurs in a relatively short time. Scour depths measured from a few very long duration experiments, as long as 10 days, were compared with scour depths from shorter duration experiments to establish criteria for extrapolating equilibrium scour depths from short duration data. Techniques for extrapolating short-duration scour measurements was the topic of the 1998 ASCE paper by Bertoldi, et al.[1]

For the conditions used in these experiments, the following percentages of equilibrium scour depths were used to extrapolate short duration scour measurements.

Approximately 75% of equilibrium scour occurred in the first 24 hours.
Approximately 81% of equilibrium scour occurred in the first 48 hours
Approximately 90% of equilibrium scour occurred in the first 72 hours
Approximately 100% of equilibrium scour occurred after 8 days.

Extrapolations from 24-hour measurements are much less reliable than extrapolations from 48-hour or longer measurements. Unfortunately most of the experiments in this study were 24-hour experiments.

Computation of Approach Flow Shear Stress

An underlying consideration in this study was that one could compute and/or measure the shear stress in the unobstructed approach flow whereas it is nearly impossible to calculate or measure shear stress in the chaotic flow region immediately in front of a pier. The notion was that we could use laboratory experiments to determine an amplification factor to be applied to the computed approach flow shear stress as an indirect measure of the shear stress in the vicinity of a pier.
Even in the relatively orderly approach flow, there are a number of ways to compute the shear stress.
The average bed shear stress in a segment of flow can be derived from Newton's first law of physics. The simplest derivation is for a segment of closed conduit flow as illustrated in figure 2.

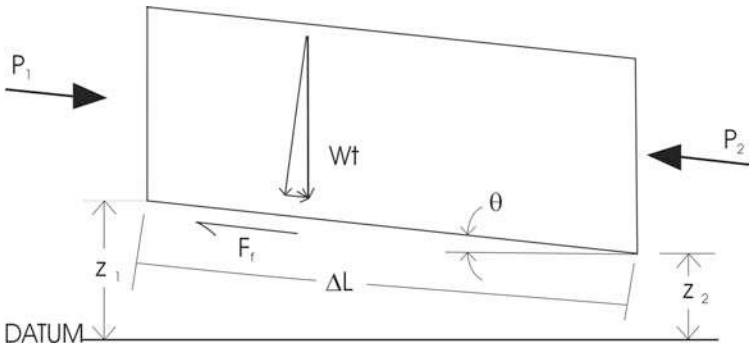

Figure 2. Free Body Diagram of Forces on a Segment of Closed Conduit Flow

$\Sigma F_x = m\ a_x$

$P_1 - P_2 - F_f + Wt \sin\theta = m\ a_x = \rho Q\ (V_2 - V_1)$

$p_1A_1 - p_2A_2 - \tau\ WP\ \Delta L + \gamma\ 1/2(A_1 + A_2)\ \Delta L \sin\theta = \rho Q\ (V_2 - V_1)$

but $A_1=A_2=A$ and $V_1= V_2$

$p_1 - p_2 - \tau\ WP/A\ \Delta L + \gamma\ \Delta L \sin\theta = 0$

$\tau = \gamma\ A/WP\ (\Delta p/\gamma + \Delta L \sin\theta)/\Delta L = 0$

but $A/WP = R_H$; $\Delta L \sin\theta = \Delta Z$; $(\Delta p/\gamma + \Delta Z) = H_{Lf}$; $H_{Lf}/\Delta L = S_F$

Substitution and simplifying yields the familiar expression for average boundary shear stress

$$\tau = \gamma R_H S_F$$

where: τ = average boundary shear stress

R_H = Hydraulic Radius = A/WP = Area / Wetted Perimeter

S_F = friction slope

Chow used a little more algebraic manipulation to derive the same expression for the average boundary shear stress in a segment of gradually varied open channel flow in a unit channel width as illustrated in figure 3.

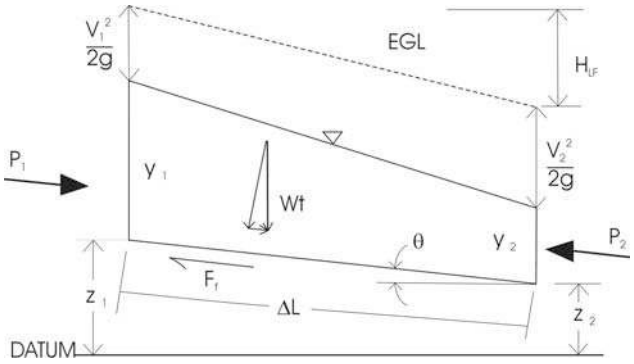

Figure 3. Free Body Diagram of Forces on a Segment of Gradually Varied Open Channel Flow

$\Sigma F_x = m\, a_x$

$P_1 - P_2 - F_f + Wt \sin\theta = m\, a_x = \rho Q\,(V_2 - V_1)$

But,

$P_1 = \tfrac{1}{2}\,\gamma\,(1)\,y_1^2$; $P_2 = \tfrac{1}{2}\,\gamma\,(1)\,y_2^2$;

$$Q = A_{AVG}\,V_{AVG} = \frac{(1)\times(y_1 + y_2)}{2}\times\frac{V_1 + V_2}{2}$$

$$Wt = \gamma \times (1)\left(\frac{y_1 + y_2}{2}\right)\Delta L$$

Substitution yields

$\tfrac{1}{2}\,\gamma\,(y_1^2 - y_2^2) - \tau\, WP\, \Delta L + \tfrac{1}{2}\,\gamma\,(y_1 + y_2)\,\Delta L \sin\theta = \rho\,[\tfrac{1}{2}\,(y_1 + y_2)\,\tfrac{1}{2}\,(V_1 + V_2)]\,(V_2 - V_1)$

Recall: $(y_1^2 - y_2^2) = (y_1 + y_2)\,(y_1 - y_2)$

Then,

$$y_1 - y_2 - \frac{\tau \times WP \times \Delta L}{\gamma\ (y_1 + y_2)/2} + \Delta L \sin\theta = 1/2\,\frac{\rho}{\gamma}\left(V_2^2 - V_1^2\right) = \frac{V_2^2}{2g} - \frac{V_1^2}{2g}$$

But, $\Delta L \sin\theta = \Delta Z = Z_1 - Z_2$

Rearranging and simplifying yields

$$\tau = \gamma\, R_H \left\{\left[\frac{V_1^2}{2g} + y_1 + Z_1\right] - \left[\frac{V_1^2}{2g} + y_2 + Z_2\right]\right\} / \Delta L = \gamma\, R_H\ H_{Lf} / \Delta L$$

$$\boxed{\tau = \gamma R_H\, S_F}$$

The obvious way to measure the approach shear stress would be very precisely measure the total energy head at two sections of flow on each side of the point of interest. Then one could compute the friction slope and shear stress from the laws of physics. However we did not take such precise measurements for these experiments. We recorded depth averaged approach velocities and approach flow depths in gradually varied flow. To compute shear stresses from the recorded average approach velocity we assumed a log velocity distribution.

Annandale proposed an erodibilty index method for estimating scour limits in rock formations.[5] He expressed average stream power in one dimensional flow as

$$SP = \gamma q S_F = \gamma V y S_F = \tau V$$

Shear stress is related to velocity squared, stream power is related to velocity cubed and it follows that shear stress is proportional to stream power raised to the exponent 2/3. Annandale later derived stream power decay equations from data provided by the TFHRC Hydraulic lab that is represented in this paper. Annandale's equations were:

$$\frac{SP_{pier}}{SP_{appr}} = 3.30\left(\frac{y_s}{y_{s\,max}}\right)^2 - 9.66\left(\frac{y_s}{y_{s\,max}}\right) + 7.66 \qquad \text{for circular piers}$$

$$\frac{SP_{pier}}{SP_{appr}} = 11.64\left(\frac{y_s}{y_{s\,max}}\right)^2 - 22.71\left(\frac{y_s}{y_{s\,max}}\right) + 12.61 \quad \text{for rectangular piers}$$

Where: SP_{pier} = max stream power around the pier at scour depth y_s
SP_{appr} = stream power in the approach flow
y_s = scour depth
$y_{s\,max}$ = maximum scour that would occur in a sand bed channel . Annandale suggested using the FHWA HEC-18 pier scour to estimate this term

At zero scour Annandale's equations indicate that the approach flow stream power is amplified around the pier by 7.66 for circular piers and by 12.61 for rectangular piers. Assuming that the shear stress is proportional to the stream power raised to the 2/3 exponent, it follows that the corresponding shear stress amplifications would be 3.9 and 5.4.

Purpose of this Paper

Data for this paper is the same as the data provided to Annandale for his analysis. This paper will evaluate shear stresses whereas Annandale was interested in stream power for the erodibility index method. Moreover the data behind the analyses have never been published. The data includes some long duration experiments that are not likely to be repeated. Part of the purpose of this paper is to make that data and the logic we used in presenting the results available for other researchers to use and build upon.

Experimental Procedure

Moveable bed experiments were conducted in the six-foot wide by seventy-foot long Tilting flume in the FHWA hydraulics lab located in McLean, Virginia. Four different sediment sizes and four pier models were used in the experiments. Sediment sizes were 0.3mm, 1.2mm, 2.4mm and 5mm. Pier models were a 152 mm (6 inch) diameter cylindrical pier, a 152 mm by 152 mm (6 inch by 6 inch) square pier, a 75mm by 300 mm (3 inch by12 inch) round nose oblong pier and a 75 mm by 300 mm (3 inch by12 inch) rectangular pier. The round nose oblong and rectangular piers were tested at 0^o, 15^o, and 30^o skew angles. The approach velocity was varied for each experiment, but it was always at or below the critical incipient motion velocity for the sediment

$$\frac{V}{U_*} = 5.75 \; \text{Log} \; \left(\frac{12.27 \; x \; y_0}{K_s}\right)$$

where: V = depth averaged velocity
U_* = shear velocity = $(\tau/\rho)^{1/2}$
y_0 = flow depth
K_s = grain roughness, use $K_s = D_{50}$ for uniform grain sizes
x = viscosity correction factor found in figure 2.97 of ASCE Manual No. 54

We fit several functions to the correction factor graph in figure 2.97 to facilitate T&E solution to determine τ from the above equation on a spreadsheet.

There are other methods such as Manning-Strickler and Moody to estimate the shear stress in the approach flow but we selected the assumed log velocity distribution to estimate shear stress from the data we recorded.

Computation of Shear Stress at the Pier

The second assumption was that the shear stress at the pier in the bottom of the scour hole must be the "effective" incipient motion (critical) shear stress when the scour hole reached equilibrium. We could assume critical shear stress at the pier when the scour depth reached equilibrium. All of the experiments were clear water experiments, which meant the approach flow shear stress was always less than critical; therefore there was always some amplification of the shear stress at the pier**.** The key word here is "effective" because one can argue that there are a lot more forces than boundary shear stresses that determine when particles could no longer get washed out of the scour hole. Our rational was that we were simply letting the sand particles tell us when all these forces were in balance and using a computed shear stress as an indicator of the balance.

The logistical problem was duration of experiments to reach equilibrium scour for clear water experiments. Theoretically clear water scour never reaches equilibrium but we found that practical equilibrium was reached in several days and we could use the trends from a few long duration tests to extrapolate scour depths from shorter duration experiments.

Shields diagram was used to compute the critical shear stress, which we assumed was the equilibrium condition in the bottom of the scour hole. Shields dimensionless shear stress is usually taken as a constant for boundary Reynolds numbers greater than 1000. Most of our laboratory experiments however had boundary Reynolds numbers in the range from 30 to 330. To facilitate computations we fit a regression equation to the portion of Shields diagram that we used. The equation

$$\tau_* = 0.0215\, R_*^{0.1585} \qquad \text{if } 10 < R_* < 700$$

where: τ_* = Shields dimensionless shear stress

R_* = Shields boundary Reynolds number

fits the Shield's diagram quite
well for our range of data.
But,

$$\tau_* = \frac{\tau_C}{(\gamma_S - \gamma) D_{50}}$$

$$R_* = \frac{\sqrt{\tau_c / \rho}\, D_{50}}{\nu}$$

where: γ = unit weight of water = 9.79 N/m^3 at 20^o C ; γ_S= 2.65 γ

ρ = mass density of water = 998 Kg/m^3 at 20^o C

υ = dynamic viscosity of water = 1.00 x 10^{-6} at 20^o C

Combining the above three expressions yields the following equation which could be solved directly for the critical shear stress:

$$\tau_c = \left[\frac{[0.0215\ \ (\gamma_S - \gamma)\, D_{50}]}{\left(\sqrt{\rho}\ \nu\right)^{0.1585}} \right]^{1.086}$$

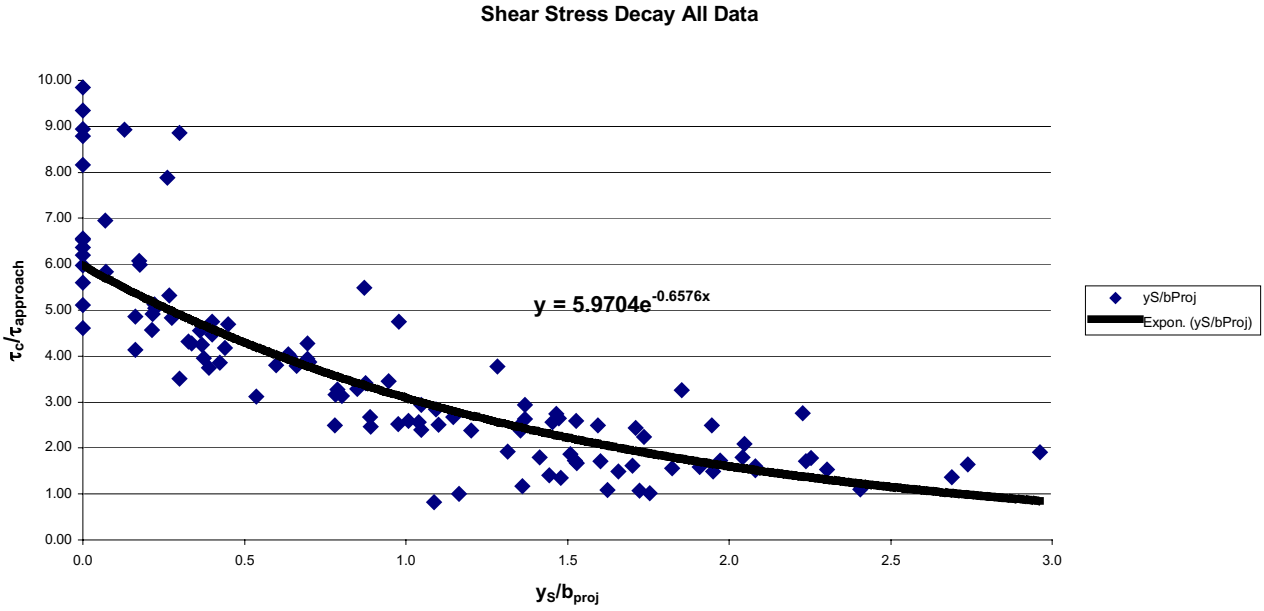

The Reynolds number, R_*, was checked for each line in the spreadsheet to ascertain that it was between 10 and 700.

Results

The ratio of critical shear stress to the approach shear stress, which was always less than critical due to the nature of the experiments, was the amplification ratio caused by the pier. The next step was to determine the equilibrium scour depth where the critical shear stress assumption was valid. A few long duration tests were run for as long as 8 days; for those tests the measured scour depth was the equilibrium scour depth. The equilibrium scour depths for shorter duration tests by extrapolating the measured scour depths as described in the 1998 ASCE paper by Bertoldi, et al.[1] We recognized that the extrapolations were not so reliable for the 24 hour tests and should have run all experiments for at least 48 hours.
Several parameters were tried for normalizing the scour depths so that the dimensionless shear stress ratio could be plotted against a dimensionless scour depth parameter. The normalizing parameter selected for this paper is the pier width so that a plot of $\tau_c/\tau_{Approach}$ vs. y_s/b could represent the shear stress amplification-decay as the scour depth got deeper. For skewed piers the projected width of the pier was used instead of the width b.

Figure 4 is a plot of all the data including round nose and rectangular piers skewed to the flow with no consideration for shape effects. It shows that the average amplification at zero scour depth is approximately 6.0. The particles tell us that the approach shear stress is amplified by a factor of six at zero scour. The amplification reduces to 1.0 at scour depths approximately 2.4 times the projected pier width. The scatter in the data can be explained in part by the large number of 24-hour tests that were in the data set.

Figure 4. Shear Stress amplification-Decay Curve for all Data

Figure 5 is a plot of circular and square piers only. It shows that the amplification is distinctly higher for the square piers than it is for circular. Figure 5 includes a single point

from exploratory PIV measurements, which are described below. The PIV point is very consistent with the indirect measurements but that came only after much discussion about how to interpret the PIV results.

were “clear water”.

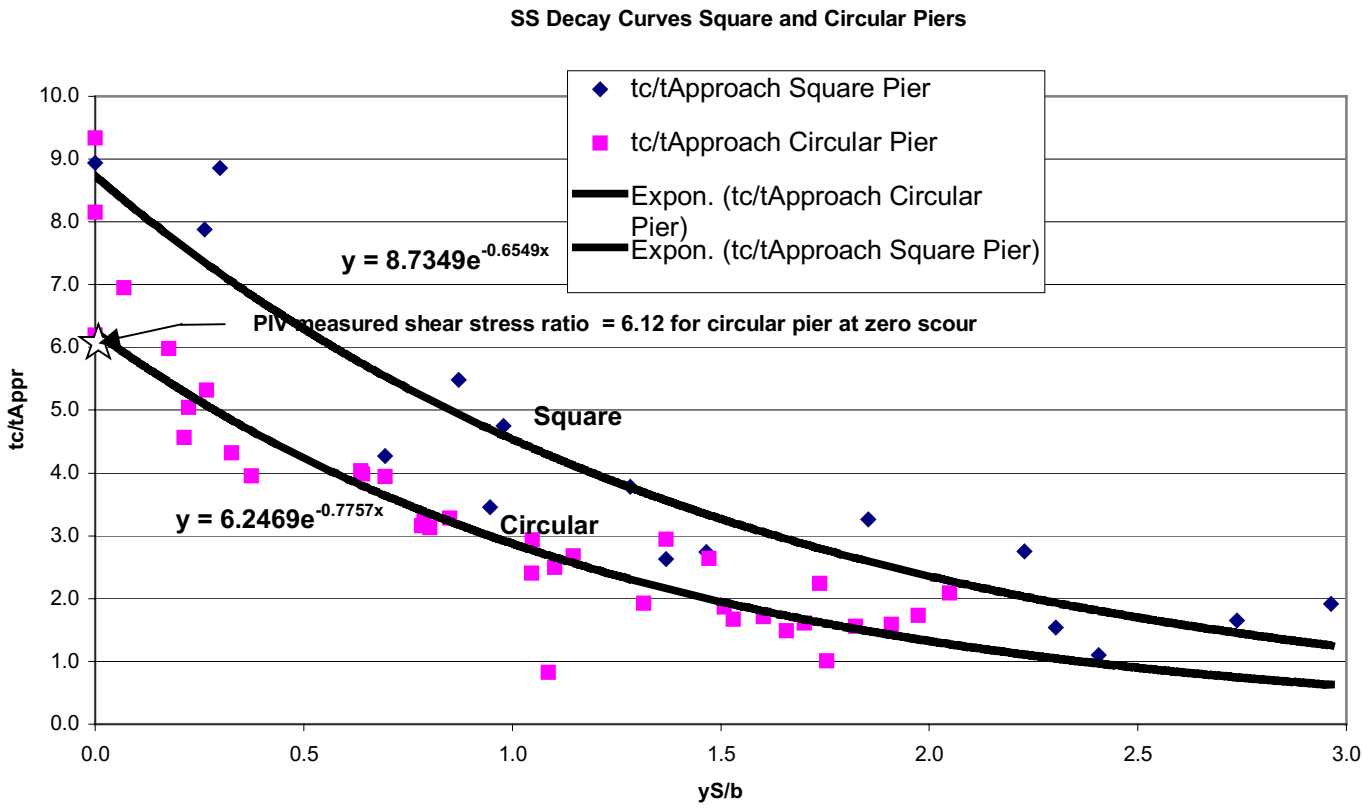

Figure 5. Shear Stress amplification-Decay Curve for Circular and Square Piers

PIV Shear Stress Measurements

Particle Image Velocimetry (PIV) is a powerful laboratory technique that utilizes laser light sheets to illuminate tracer particles in the water and high-speed digital cameras to quantify velocity fields in an experimental set-up. Researchers at the TFHRC hydraulics lab have been developing this technology as a tool for explaining some of the scour

processes we observe. We made small-scale exploratory tests to measure velocity fields very close to the boundary and compute the theoretical shear stresses as a check for the indirect measurements we made with the moveable bed scour tests. If this method works, we can accelerate the tests considerably and establish a sound theoretical basis for the results. The advantage of this method is we could perform fixed bed scour holes and test a wide range of approach flow condition to validate an inherent assumption that the **ratio** of shear stresses holds for a wide range of approach flow velocities.

The theoretical shear stress at any point in a two dimensional flow field is made up of two components- the laminar component and the turbulent component as follows:

$$\tau = \mu\left[\frac{\partial \bar{u}}{\partial y} + \frac{\partial \bar{v}}{\partial x}\right] - \rho\overline{u'v'}$$

where: The first term on the right side is the laminar component and the second term is the turbulent component

u and v are point velocities in the x and y directions respectively

u' and v' are the turbulent fluctuations

Since PIV can measure all of these quantities at discrete pixels in the flow field, it seemed reasonable that the shear stresses could be calculated from a PIV flow field. The partial derivatives are evaluated by computing the incremental changes at adjacent pixels

Figure 6 is the PIV velocity field measured in front of a very small model of a bridge pier. Figure 7 is the zoomed view of the velocity field and resulting shear stress distribution immediately upstream of the pier where vorticity seemed strongest.

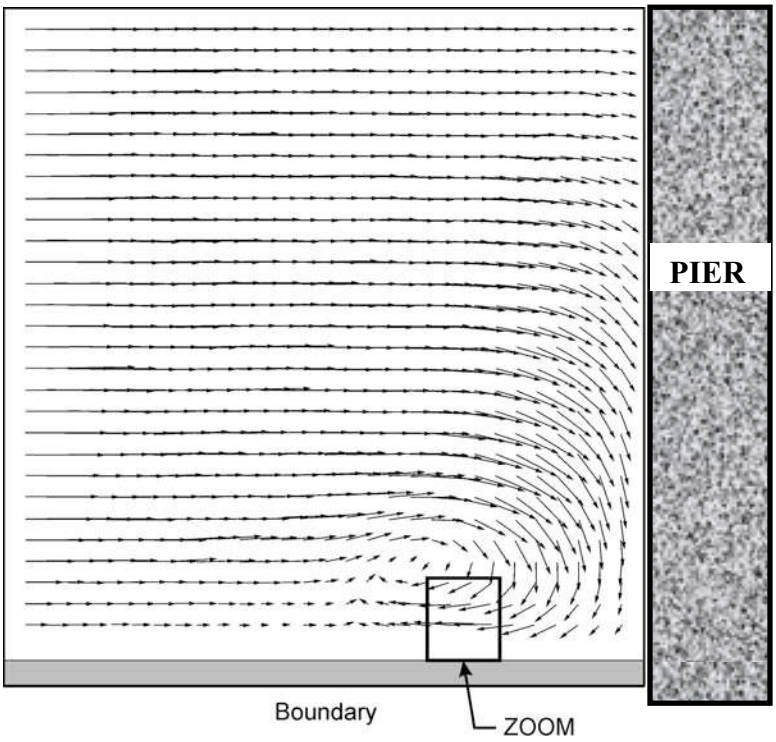

Figure 6. PIV velocity field upstream of a bridge pier model

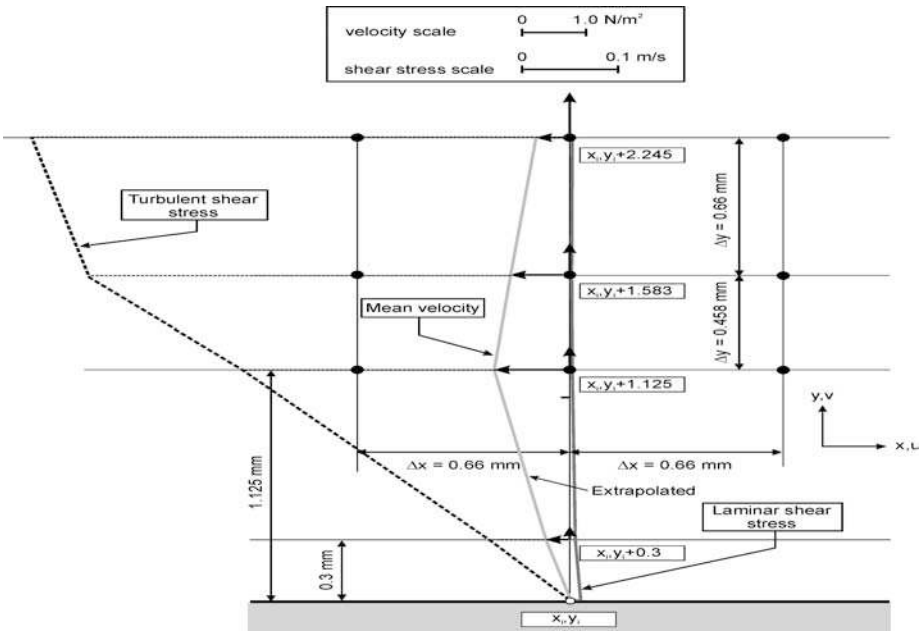

Figure 7. Zoomed Velocity Field and Shear Stress Distribution Near the Bed

The laminar shear stresses at the bed dominate in the approach flow and the turbulent shear stresses dominate in front of the pier as indicated in table 1. The problem we had was where to form the ratio because the turbulent shear stress must go to zero at a no slip boundary. If we compared shear stresses right at the bed , it would appear that the ratio was less than1.0 even at zero scour. If we compared shear stresses at the first measured pixel,which was 1.125 mm above the bed it would appear that the amplification was approximately 95. But if we extrapolated the shear stresses to a close proximity to the bed, 0.33 mm, equal to the diameter of the smallest particles used in the scour tests, then the ratio was a reasonable value of 6.15. That value was plotted on figure 5.
PIV shows promise but we need more experience to apply it to this problem. Perhaps better lens and larger scale tests will eliminate skepticism, but without the indirect measurements from the scour tests as a gage, we may never have reached a reasonable conclusion from these PIV results.

Table1. PIV Shear Stress Results

Approach Flow						
x_i	y_i	$\overline{u}$ [m/s]	$\overline{v}$ [m/s]	$\rho\overline{u'v'}$ [N/m²]	$\mu\left(\frac{\partial\overline{u}}{\partial y}+\frac{\partial\overline{v}}{\partial x}\right)$ [N/m²]	τ_{TOT} [N/m²]
x_i	$y_i + 0$	0	0	0	.254	0.254
x_i	$y_i + 0.3$	.562	0	-.0115	.21411	0.22561
x_i	$y_i + 1.125$	.213	0	-.0277	.0322	0.0599
x_i	$y_i + 1.583$	.234	0	-.019	.0389	0.0579
x_i	$y_i + 2.245$	.265	0	-.0076	.0424	0.05
In Front of Pier						

x_i	y_i	$\overline{u}$ [m/s]	$\overline{v}$ [m/s]	$\rho\overline{u'v'}$ [N/m^2]	$\mu\left(\frac{\partial\overline{u}}{\partial y}+\frac{\partial\overline{v}}{\partial x}\right)$ [N/m^2]	τ_{TOT} [N/m^2]
x_i	$y_i + 0$	0	0	0	.1366	0.1366
x_i	$y_i + 0.3$	-.024	.0114	-1.297	.0907	1.3877
x_i	$y_i + 1.125$	-.078	.0376	-5.098	.0168	5.1148
x_i	$y_i + 1.583$	-.0624	.0516	-6.606	.0296	6.6356
x_i	$y_i + 2.245$	-.0338	.0727	-8.446	.0480	8.494

Conclusions

Shear stress is a key to estimating scour at bridge piers especially in cohesive bed materials, but shear stresses are very difficult to quantify in the chaotic flow field in front of bridge piers.

This paper presents a simple but tedious technique for quantifying shear stresses by using sand particles as an indirect measure.

PIV shows promise as a more theoretical technique for quantifying shear stresses but we need further development and experience.

The indirect measure described in this paper will serve as a gage for more the interpretation of numerical and physical model results that may have a more theoretical basis.

References

1. Bertoldi, David A. and J. Sterling Jones, "Time to Scour Experiments as an Indirect Measure of Stream Power Around Bridge Piers." Proceedings of the ASCE International Water Resources Engineering Conference held in Memphis, TN, pp 264-269, 1998.
2. Johnson, Peggy A. and J. Sterling Jones, "Shear Stress at Base of Bridge Pier," Transportation Research Record No. 1350, Transportation Research Board, pp 14-18, 1992.
3. Parola, A.C., "The Stability of Riprap Used to Protect Bridge Piers," Publication No. FHWA-RD-91-063, Federal Highway Administration, Office of Research and Development, 1991
4. Pagan, Jorge, "Stability of Riprap for Protection at the Toe of Abutments," Publication No. FHWA-RD-91-057, Federal Highway Administration, Office of Research and Development, 1991
5. Annandale, George W., "Calculation of Pier Scour Using the Erodibility Index Method," Draft notes for a short course presented to the Maryland State Highway Administration, April 1999.
6. Annandale, George W. and Steve P. Smith, "Proposed Pier Scour Procedure for Rock Formations" Proceedings of the ASCE International Water Resources Engineering Conference held in Memphis, TN, pp 258-263, 1998.

Appendix Summary of Data

Run #	Run Time (hrs)	Description	Skew Angle (degrees)	b_{proj} (mm)	D_{50} (mm)	Flow Depth y_a (m)	Approach Velocity Va (m/s)	Measured Scour Depth y_s (m)	Estimated Equilibrium Scour Depth y_{equil} (m)	Einstein Barborosa Approach Shear Stress τ_a (N/m^2)	τ_c (N/m^2)	τ_c/τ_a	y_S/b_{Proj}
45	24	Square Pier	0	152	1.2	0.267	0.520	0.274	0.366	0.657	0.723	1.10	2.41
30	72	152mm x 152mm	0	152	1.2	0.267	0.443	0.315	0.350	0.470	0.723	1.54	2.30
56R	41		0	152	1.2	0.267	0.344	0.166	0.208	0.275	0.723	2.63	1.37
31	72		0	152	1.2	0.267	0.337	0.201	0.223	0.264	0.723	2.74	1.47
46	24		0	152	1.2	0.267	0.301	0.108	0.144	0.209	0.723	3.46	0.95
6	23.3		0	152	1.2	0.267	0.272	0.079	0.106	0.169	0.723	4.27	0.70
136	24		0	152	1.2	0.305	0.204	0.030	0.040	0.092	0.723	7.88	0.26
5	1	Incipient scour at pier	0	152	1.2	0.267	0.189	0.000	0.000	0.081	0.723	8.94	0.00
15	24	Circular Pier	0	152	1.2	0.267	0.541	0.200	0.267	0.713	0.723	1.01	1.75
47	24	152mm x 152mm	0	152	1.2	0.267	0.442	0.208	0.277	0.465	0.723	1.56	1.82
52R	24		0	152	1.2	0.267	0.434	0.194	0.258	0.449	0.723	1.61	1.70
134	72		0	152	1.2	0.267	0.422	0.219	0.244	0.422	0.723	1.71	1.60
49	24		0	152	1.2	0.267	0.352	0.126	0.167	0.289	0.723	2.50	1.10
57R	144		0	152	1.2	0.267	0.340	0.174	0.174	0.270	0.723	2.68	1.15
50	70		0	152	1.2	0.267	0.310	0.108	0.120	0.221	0.723	3.27	0.79
10	23.3		0	152	1.2	0.267	0.270	0.037	0.050	0.167	0.723	4.32	0.33
135	6		0	152	1.2	0.267	0.230	0.020	0.027	0.121	0.723	5.98	0.18
48	1	Incipientscour at pier	0	152	1.2	0.267	0.185			0.077	0.723	9.34	0.00
41	24	Round Nose Pier	0	75	1.2	0.267	0.526	0.097	0.129	0.671	0.723	1.08	1.72
42	24	75mm x 300mm	0	75	1.2	0.267	0.446	0.117	0.156	0.475	0.723	1.52	2.08
54R	24		0	75	1.2	0.267	0.435	0.117	0.156	0.451	0.723	1.60	2.08
40	67		0	75	1.2	0.267	0.352	0.090	0.101	0.290	0.723	2.49	1.35
44	70		0	75	1.2	0.267	0.303	0.059	0.066	0.212	0.723	3.42	0.88
20	23.3		0	75	1.2	0.267	0.258	0.023	0.030	0.152	0.723	4.75	0.40
16	1	Incipient	0	75	1.2	0.267	0.238			0.129	0.723	5.60	0.00
43	24	Round Nose Pier	15	150.09	1.2	0.267	0.524	0.183	0.244	0.667	0.723	1.08	1.62
29	48	75mm x 300mm	15	150.09	1.2	0.267	0.419	0.192	0.229	0.417	0.723	1.73	1.52
28	24		15	150.09	1.2	0.267	0.273	0.041	0.055	0.170	0.723	4.25	0.37
137	6		15	150.09	1.2	0.267	0.263	0.041	0.054	0.159	0.723	4.55	0.36
23	1	Incipient scour at pier	15	150.09	1.2	0.267	0.249			0.141	0.723	5.12	0.00
53R	24	Round Nose Pier	30	214.95	1.2	0.267	0.544	0.188	0.250	0.720	0.723	1.00	1.16
38	24	75mm x 300mm	30	214.95	1.2	0.267	0.505	0.219	0.293	0.616	0.723	1.17	1.36
39	24		30	214.95	1.2	0.267	0.413	0.228	0.304	0.403	0.723	1.79	1.41

Run #	Run Time (hrs)	Description	Skew Angle (degrees)	b_{proj} (mm)	D_{50} (mm)	Flow Depth y_a (m)	Approach Velocity Va (m/s)	Measured Scour Depth y_s (m)	Estimated Equilibrium Scour Depth y_{equil} (m)	Einstein Barborosa Approach Shear Stress τ_a (N/m^2)	τ_c (N/m^2)	τ_c/τ_a	y_S/b_{Proj}
35	24		30	214.95	1.2	0.267	0.348	0.168	0.224	0.283	0.723	2.56	1.04
36	24		30	214.95	1.2	0.267	0.287	0.096	0.128	0.190	0.723	3.81	0.60
37	24		30	214.95	1.2	0.267	0.266	0.065	0.086	0.161	0.723	4.48	0.40
138	24		30	214.95	1.2	0.267	0.256	0.045	0.059	0.150	0.723	4.83	0.28
34	1	Incipient scour at pier	30	214.95	1.2	0.267	0.220			0.110	0.723	6.57	0.00
58	192	Circular Pier	0	152.00	0.3	0.267	0.289	0.165	0.165	0.154	0.126	0.82	1.09
62	24	Square Pier	0	152.00	2.4	0.267	0.645	0.307	0.409	1.271	1.729	1.36	2.69
133	24	152mm x 152mm	0	152.00	2.4	0.267	0.480	0.266	0.296	0.694	1.729	2.49	1.95
85	24		0	152.00	2.4	0.267	0.485	0.195	0.260	0.711	1.729	2.43	1.71
59	24		0	152.00	2.4	0.267	0.479	0.182	0.242	0.693	1.729	2.49	1.59
60	24		0	152.00	2.4	0.267	0.387	0.080	0.106	0.447	1.729	3.87	0.70
61	72		0	152.00	2.4	0.267	0.352	0.062	0.068	0.369	1.729	4.69	0.45
130	6		0	152.00	2.4	0.267	0.257	0.018	0.020	0.194	1.729	8.93	0.13
84	1	Incipient scour at pier	0	152.00	2.4	0.267	0.259			0.197	1.729	8.79	0.00
67	24	Circular Pier	0	152.00	2.4	0.267	0.618	0.189	0.252	1.163	1.729	1.49	1.66
127	24		0	152.00	2.4	0.267	0.583	0.174	0.232	1.035	1.729	1.67	1.53
128	144		0	152.00	2.4	0.267	0.544	0.200	0.200	0.897	1.729	1.93	1.32
65	72	152mm x 152mm	0	152.00	2.4	0.267	0.488	0.143	0.159	0.720	1.729	2.40	1.05
87*	24		0	152.00	2.4	0.267	0.442	0.156	0.208	0.587	1.729	2.94	1.37
129	24		0	152.00	2.4	0.267	0.443	0.119	0.159	0.589	1.729	2.94	1.05
86	72		0	152.00	2.4	0.267	0.429	0.110	0.122	0.553	1.729	3.13	0.80
74	144		0	152.00	2.4	0.267	0.427	0.119	0.119	0.546	1.729	3.16	0.78
64	24		0	152.00	2.4	0.267	0.383	0.043	0.057	0.437	1.729	3.96	0.37
63	24		0	152.00	2.4	0.267	0.357	0.024	0.033	0.379	1.729	4.57	0.21
66	1	Incipient scour at pier	0	152.00	2.4	0.267	0.308			0.279	1.729	6.20	0.00
70	24	Round Nose	0	75.00	2.4	0.267	0.618	0.110	0.146	1.163	1.729	1.49	1.95
132	24		0	75.00	2.4	0.267	0.490	0.076	0.102	0.724	1.729	2.39	1.35
71R	72	75mm x 300mm	0	75.00	2.4	0.267	0.490	0.081	0.090	0.724	1.729	2.39	1.20
69	24		0	75.00	2.4	0.267	0.477	0.055	0.073	0.686	1.729	2.52	0.98
72	24		0	75.00	2.4	0.267	0.368	0.019	0.025	0.404	1.729	4.28	0.34
131	6		0	75.00	2.4	0.267	0.346	0.009	0.012	0.356	1.729	4.86	0.16
68	1	Incipient scour at pier	0	75.00	2.4	0.267	0.355			0.375	1.729	4.61	0.00
73	24	Round Nose	15	150.09	2.4	0.267	0.647	0.166	0.222	1.278	1.729	1.35	1.48
75	24		15	150.09	2.4	0.267	0.479	0.088	0.117	0.694	1.729	2.49	0.78
76	24		15	150.09	2.4	0.267	0.393	0.044	0.059	0.462	1.729	3.75	0.39

Run #	Run Time (hrs)	Description	Skew Angle (degrees)	b_{proj} (mm)	D_{50} (mm)	Flow Depth y_a (m)	Approach Velocity Va (m/s)	Measured Scour Depth y_s (m)	Estimated Equilibrium Scour Depth y_{equil} (m)	Einstein Barborosa Approach Shear Stress τ_a (N/m^2)	τ_c (N/m^2)	τ_c/τ_a	y_S/b_{Proj}
78	24		15	150.09	2.4	0.267	0.337	0.025	0.033	0.337	1.729	5.13	0.22
77	1	Incipient scour at pier	15	150.09	2.4	0.267	0.304			0.271	1.729	6.37	0.00
80	24	Round Nose	30	214.95	2.4	0.267	0.634	0.233	0.310	1.224	1.729	1.41	1.44
81	72	75mm x 300mm	30	214.95	2.4	0.267	0.481	0.173	0.192	0.700	1.729	2.47	0.89
82	24		30	214.95	2.4	0.267	0.387	0.068	0.091	0.448	1.729	3.86	0.42
83	24		30	214.95	2.4	0.267	0.344	0.035	0.046	0.352	1.729	4.91	0.22
79	1	Incipient scour at pier	30	214.95	2.4	0.267	0.313			0.289	1.729	5.98	0.00
123	24	Square Pier	0	152.00	5	0.267	0.833	0.312	0.416	2.644	4.354	1.65	2.74
99	24	152mm x 152mm	0	152.00	5	0.267	0.773	0.338	0.450	2.275	4.354	1.91	2.96
98	72		0	152.00	5	0.267	0.644	0.305	0.339	1.581	4.354	2.75	2.23
124	72		0	152.00	5	0.267	0.592	0.254	0.282	1.336	4.354	3.26	1.85
100	24		0	152.00	5	0.267	0.550	0.146	0.195	1.152	4.354	3.78	1.28
90	24		0	152.00	5	0.267	0.491	0.112	0.149	0.917	4.354	4.75	0.98
89	24		0	152.00	5	0.267	0.457	0.099	0.132	0.794	4.354	5.48	0.87
122	6		0	152.00	5	0.267	0.359	0.034	0.046	0.491	4.354	8.86	0.30
88	1	Incipient scour at pier	0	152.00	5	0.267	0.316			0.378	4.354	11.51	0.00
96	24	Circular Pier	0	152.00	5	0.267	0.847	0.218	0.290	2.733	4.354	1.59	1.91
121	24	152mm x 152mm	0	152.00	5	0.267	0.813	0.225	0.300	2.516	4.354	1.73	1.97
125	144		0	152.00	5	0.267	0.784	0.229	0.229	2.337	4.354	1.86	1.51
97	24		0	152.00	5	0.267	0.740	0.233	0.311	2.084	4.354	2.09	2.05
126	144		0	152.00	5	0.267	0.713	0.264	0.264	1.937	4.354	2.25	1.74
95	28		0	152.00	5	0.267	0.658	0.170	0.224	1.648	4.354	2.64	1.47
109	144		0	152.00	5	0.267	0.590	0.129	0.129	1.325	4.354	3.29	0.85
120	72		0	152.00	5	0.267	0.535	0.088	0.098	1.091	4.354	3.99	0.64
94	72		0	152.00	5	0.267	0.539	0.095	0.106	1.105	4.354	3.94	0.70
93	24		0	152.00	5	0.267	0.532	0.073	0.097	1.079	4.354	4.04	0.64
110	6		0	152.00	5	0.267	0.476	0.026	0.034	0.863	4.354	5.04	0.22
92	24		0	152.00	5	0.267	0.464	0.030	0.041	0.818	4.354	5.32	0.27
111	6		0	152.00	5	0.267	0.406	0.008	0.011	0.626	4.354	6.95	0.07
91	1	Incipient scour at pier	0	152.00	5	0.267	0.375			0.534	4.354	8.15	0.00
104	24	Round Nose	0	75.00	5	0.267	0.800	0.127	0.169	2.436	4.354	1.79	2.25
103	72	75mm x 300mm	0	75.00	5	0.267	0.635	0.074	0.082	1.534	4.354	2.84	1.09
119	24		0	75.00	5	0.267	0.571	0.020	0.022	1.240	4.354	3.51	0.30
102	24		0	75.00	5	0.267	0.526	0.009	0.012	1.054	4.354	4.13	0.16
101	1	Incipient	0	75.00	5	0.267	0.419			0.667	4.354	6.53	0.00

Run #	Run Time (hrs)	Description	Skew Angle (degrees)	b_{proj} (mm)	D_{50} (mm)	Flow Depth y_a (m)	Approach Velocity Va (m/s)	Measured Scour Depth y_s (m)	Estimated Equilibrium Scour Depth y_{equil} (m)	Einstein Barborosa Approach Shear Stress τ_a (N/m^2)	τ_c (N/m^2)	τ_c/τ_a	y_S/b_{Proj}
107	24	Round Nose	15	150.09	5	0.267	0.797	0.230	0.306	2.418	4.354	1.80	2.04
108	72	75mm x 300mm	15	150.09	5	0.267	0.654	0.120	0.133	1.628	4.354	2.67	0.89
106	24		15	150.09	5	0.267	0.524	0.049	0.066	1.044	4.354	4.17	0.44
118	6		15	150.09	5	0.267	0.434	0.020	0.026	0.717	4.354	6.07	0.17
105	1	Incipient scour at pier	15	150.09	5	0.267	0.341			0.442	4.354	9.85	0.00
114	24	Round Nose	30	214.95	5	0.267	0.817	0.361	0.481	2.539	4.354	1.71	2.24
115	72	75mm x 300mm	30	214.95	5	0.267	0.668	0.281	0.312	1.699	4.354	2.56	1.45
117	24		30	214.95	5	0.267	0.665	0.246	0.328	1.684	4.354	2.59	1.53
112	24		30	214.95	5	0.267	0.550	0.107	0.142	1.151	4.354	3.78	0.66
116	6		30	214.95	5	0.267	0.443	0.012	0.015	0.746	4.354	5.84	0.07
113	1	Incipient scour at pier	30	214.95	5	0.267	0.326			0.403	4.354	10.81	0.00